MDPI

Article

The Effect of Heat Treating and Deformation by Rolling and Forging on the Mechanical Properties of the 4032-Type Alloy Prepared from Recycled Materials

José Ivan Valencia de Lima * , Francisco Alfredo García Pastor and Alfredo Flores Valdés

Centro de Investigación y de Estudios Avanzados del Instituto Politécnico Nacional, Avenida Industria Metalúrgica Número 1062, Ramos Arizpe 25900, Saltillo Coahuila, Mexico; francisco.garcia@cinvestav.edu.mx (F.A.G.P.); alfredo.flores@cinvestav.edu.mx (A.F.V.)
* Correspondence: ivan.valencia@cinvestav.edu.mx; Tel.:+52-2223452075

Abstract: In the present work, the relationship between deformation, microstructure and mechanical properties of the Sr-modified 4032-type eutectic aluminum alloy was studied. The alloy was prepared from recycled materials, mainly from maritime and automotive 356 alloy scrap samples. Solubilizing heat treatment was carried out at a temperature of 450 °C with a holding time of 8 h. Finally, different samples were subjected to rolling and forging processes at a temperature of 450 °C, thus achieving a reduction of 25% of the original thickness. As expected, the microstructure and properties changed significantly due to the deformation processes, where an important factor was the change in the morphology of eutectic silicon, not only produced by the application of deformation, but also on the effect of adding strontium as a modifying agent. The samples were characterized by optical microscopy and scanning electron microscopy, where it was possible to observe not only the effect of strontium on the morphology of eutectic silicon but also the effect of the heat treatment performed. The tensile tests showed that there was indeed a notable increase in the ultimate tensile stress, yield strength, and resistance to fracture, while initial hardness also considerably increased. Finally, the fracture analysis showed that, after thermal treatment and deformation, all the samples analyzed presented a fracture within the ductile regime. It was shown that the combination of deformation and the addition of strontium led to improved globulization of the eutectic silicon.

Keywords: aluminum recycling; rolling; forging; silicon microstructure and morphology

1. Introduction

Aluminum-based alloys have interesting properties such as high corrosion resistance, high ductility, good thermal and electrical conductivity, and high chemical stability coupled with relatively low density when compared to steel. To improve resistance to environmental corrosion, complex electro-passivation processes are often applied to avoid pitting and grain-boundary corrosion. Worldwide, aluminum products have reached second place in terms of production volume, just below iron and steel products [1]. Another important feature of most aluminum alloys is the relative ease of being recycled, as remelting requires only 5% of the total energy required to obtain it directly from bauxite [2]. Specifically, the 4032-aluminum alloy (AA4032) is considered a high-performance aluminum alloy, which is used in industrial applications such as the elaboration of automotive and aerospace components or the manufacturing of many other miscellaneous components [3].

The presence of diverse and complex intermetallic phases is quite common in this alloy; the main elements that contribute to the formation of such intermetallic phases are Cu, Fe, Mg, Ni and Si. The composition and density of the intermetallic phases commonly found in the microstructure of a typical 4032 alloy are compared to those mentioned by Belov and collaborators [4]. Iron is an element that can be usually found in most aluminum

alloys; this element is added to improve strength and usually presents a trade-off with ductility [5].

Several works have reported the influence of the addition of modifying elements of eutectic silicon, such as Sr, Na or P; the main effect is on the mechanical properties, particularly tensile strength, which can reach significant values as compared to those of the alloy in the as-cast condition [6]. Other elements, such as Mg, promote the precipitation of the intermetallic Mg_2Si, having an η—phase well known to improve strength in a range of Al alloys, such as the 7xxx series, which has an important effect on hardness and ductility. Cu and Ni also have an important influence on both microstructure and mechanical properties, specifically after heat treatment [7].

On the other hand, thermomechanical treatments, such as equal-channel angular pressing (ECAP) [8], accumulative roll bonding (ARB) [9,10], severe plastic deformation by twist extrusion (TE), hot extruding, free forging [11] and hot rolling [12], have gained importance in the last decade. The importance of these severe plastic deformation (SPD) techniques centers on the fact that they can cause the aluminum alloy to produce a finer grain structure, which gives the alloy greater strength and/or ductility [13].

Among these deformation technologies, hot rolling and free forging tend to be relatively cheaper and simpler to perform but have a profound effect on the mechanical properties and microstructure of the alloy [14].

Temperature also has a great influence on the mechanical properties and microstructure of aluminum alloys. As mentioned by Huie Hu et al. [15], tensile strength increases rapidly at processing temperatures between 400 °C and 450 °C, while elongation decreases at temperatures above 400 °C. As for the effect of deformation temperature on the microstructure, a finer grain refinement homogeneously distributed throughout the matrix is achieved for temperatures close to 430 °C; however, at a deformation temperature close to 480 °C, the recrystallized grains undergo coarsening and therefore a not very favorable microstructure, as mentioned by Peng Sun et al. [13].

For these reasons, the objective of this work was to study the feasibility of deformation processing of aluminum alloy type 4032, where the specimens were prepared using recycled materials, studying the relationship between processing conditions and the microstructure and mechanical properties, and through digital image processing, the transformation percentage and the average circularity of the eutectic silicon were evaluated.

2. Materials and Methods

2.1. Production of Aluminum Alloy Type 4032

Samples of the 4032-type alloy were prepared from scrap and chips from 356 aluminum alloy (AA356)-type alloys, with the composition shown in Table 1. According to the reported values, the calculation for the corresponding adjustment was made using silicon lumps (99.9 wt.%), Cu wire chips (99.9 wt.%), Mg (99.9 wt.%), Al-20 wt.% Ni, and Al-15 wt.% Sr master alloys; the latter was added as a eutectic silicon modifier. The melting of the scrap was carried out in a medium frequency induction furnace in a temperature range between 750 °C to 800 °C to which the different alloying elements were added. After melting, flux was added to remove the slag and subsequently degassed with commercial purity argon for 10 min. The chemical composition of the alloy after adjustment is presented in Table 2, where the concentration of Sr was chosen according to Tebib et al. [16]. The diagram in Figure 1 shows the main stages of this process, as well as a brief description of them.

Table 1. Chemical composition of the AA356 chips and scraps used to prepare the samples used in this work.

Element	Si	Mg	Cu	Ni	Fe	Ti	Sr	Zn	Mn	Al
Quantity (wt.%)	7.52	0.25	0.08	0.06	0.24	0.11	Traces	0.03	0.01	Bal

Table 2. Chemical composition of the alloy after adjustment.

Element	Si	Mg	Cu	Ni	Fe	Ti	Sr	Zn	Mn	Al
Quantity (wt.%)	12.14	0.86	0.81	0.65	0.20	0.14	0.04	0.02	0.01	Bal
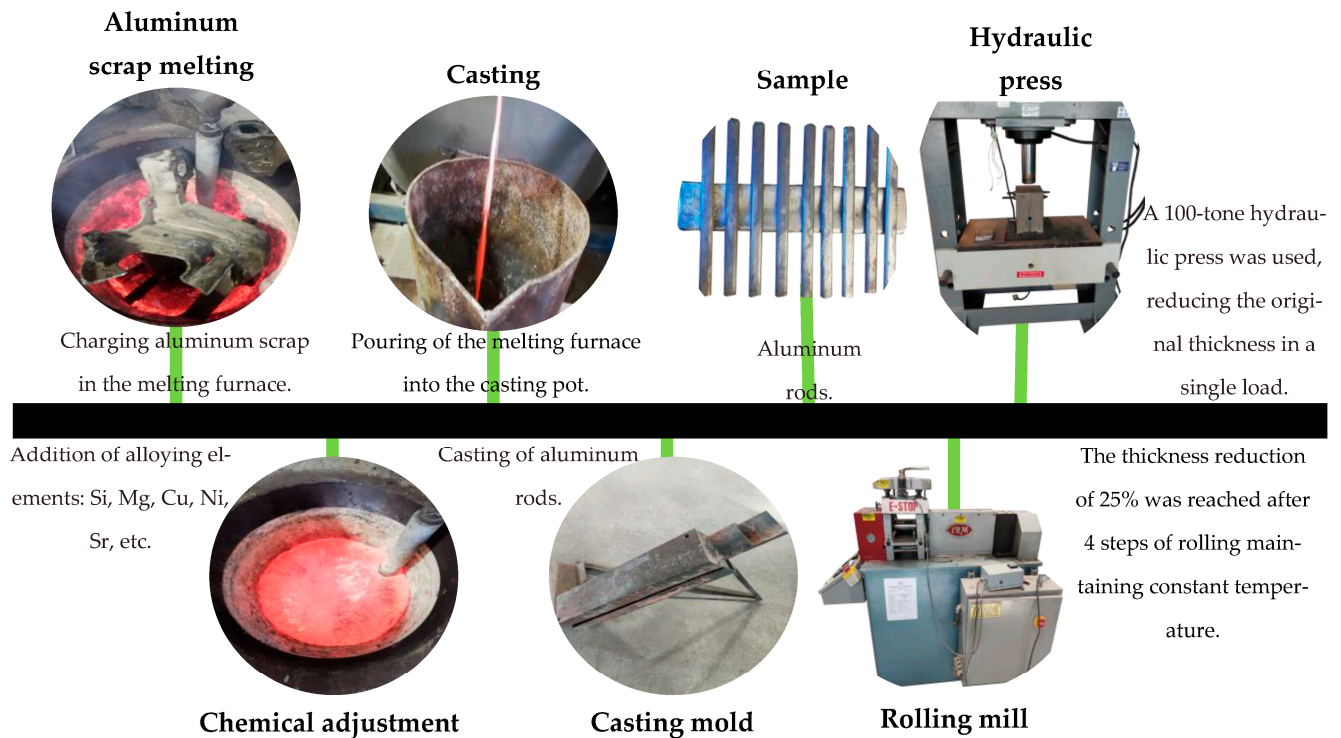
Figure 1. Illustrative diagram of the main stages of the process.

2.2. Casting and Sample Collection

To cast the samples, a zirconia-painted H13 tooling steel mold was preheated at a temperature of 350 °C, having attached a specially designed feeder. Pouring was done by manually tilting the mold, and finally after solidifying, each sample was extracted from the mold and cut according to the requirements of the scheduled mechanical tests. The cut pieces were studied under the following conditions: As-cast, heat-treated (HT) at a temperature of 450 °C for 8 h, followed by cooling to room temperature; rolled with pre-heat treatment (HT-Rolled) and a rolling temperature of 450 °C; and finally, the forged samples without/with heat pre-treatment, respectively (Forged and HT-Forged) at a forging temperature of 450 °C.

2.3. Rolling and Forging Process

Rolling was carried out in a 2-hi rolling mill (International Rolling Mills, RI, USA) equipped with D2 tool steel rollers (diameter = 10 cm) and a maximum separation force of 20 metric tons. The samples were preheated in a resistance electrical furnace at a temperature range between 420 °C to 450 °C, and according to some previous studies realized in this work, it was selected to apply a thickness reduction of 25% to obtain the best values of mechanical properties without cracking. The thickness reduction of 25% was reached after 4 steps of rolling while maintaining constant temperature (see Figure 1), where the speed of the rollers remained at 8 rpm. Figure 2 shows the thickness of the sample before/after the deformation process.

Figure 2. Cross-sectional area of the aluminum alloy sample. (**a**) Original (As-cast), (**b**) before the rolling/forging process, and (**c**) after applying the rolling/forging process.

The open forging process was carried out in the same temperature range using a 100-ton hydraulic press, reducing the original thickness of the sample by 25% in a single load (see Figure 2).

2.4. Testing and Characterization

The resultant microstructures were examined using a Vanox brand optical microscope, while some samples were observed using a PHILIPS model XL30 scanning electron microscope (SEM). In the case of the SEM analysis, backscattered electron (BSE) contrast was used to obtain maximum contrast in the phases and secondary electrons (SE) for higher resolution at higher magnifications. The stoichiometry of the alloy phases was identified by comparing the results of the dispersed energy spectroscopy (EDS) analysis with the results reported in the literature [17].

The specimens for the stress–strain tests were machined and tested (a specimen for each sample, that is 5 in total) in accordance with ASTM E8, and an MTS QTEST/100 universal test machine was used. Finally, fracture analysis was performed on the surface of these samples using SEM.

2.5. DIP Using ImageJ

For digital image processing (DIP) [18], we present the use of ImageJ software [19], which is in the public domain, for the analysis and determination of microstructural parameters in AA4032. Specifically, the software was used to measure the percentage conversion of eutectic silicon particles into more rounded particles using the circularity function. Five images were analyzed, one for each sample.

The process consisted of determining the percentage in area of the eutectic silicon present in the sample. At the same time, the average circularity of the silicon was determined, considering that those particles that had a value very close to zero were considered needles or acicular silicon; while other particles that presented values very close to one were considered globular silicon particles. The ImageJ version used for this analysis was 1.53 t, and the process was carried out considering the ImageJ manual [20], which is briefly described.

We worked with an 8-bit image format, and then the image was binarized considering the areas of interest (eutectic silicon), using the parameters chosen for the analysis: "Area" and "Shape descriptors".

Finally, a particle size range was established between 0.1 and 40 and a circularity from 0.0 to 1.0.

The circularity or form factor was calculated as follows:

$$\text{Circularity} = \frac{4\,\pi A}{p^2},\tag{1}$$

where A is the area of all particles and p represents the perimeter of the particles. This procedure was repeated for the 5 samples; the results obtained are discussed in the following section.

For the elaboration of the relative frequency histograms, the method described by David Scott was used to evaluate the optimal width of the histogram bins [21].

3. Results and Discussion

3.1. Microstructure and Characterization

Figure 3a shows the microstructure of the As-cast, consisting of elongated particles of needle-like morphology corresponding to eutectic silicon. As has been broadly discussed in the literature, this type of morphology of the eutectic silicon particles decreases the mechanical properties of the alloy [22]; as already mentioned, these negative effects can be minimized by the application of heat treatment, together with the addition in the molten state of a eutectic silicon modifying agent, such as strontium.
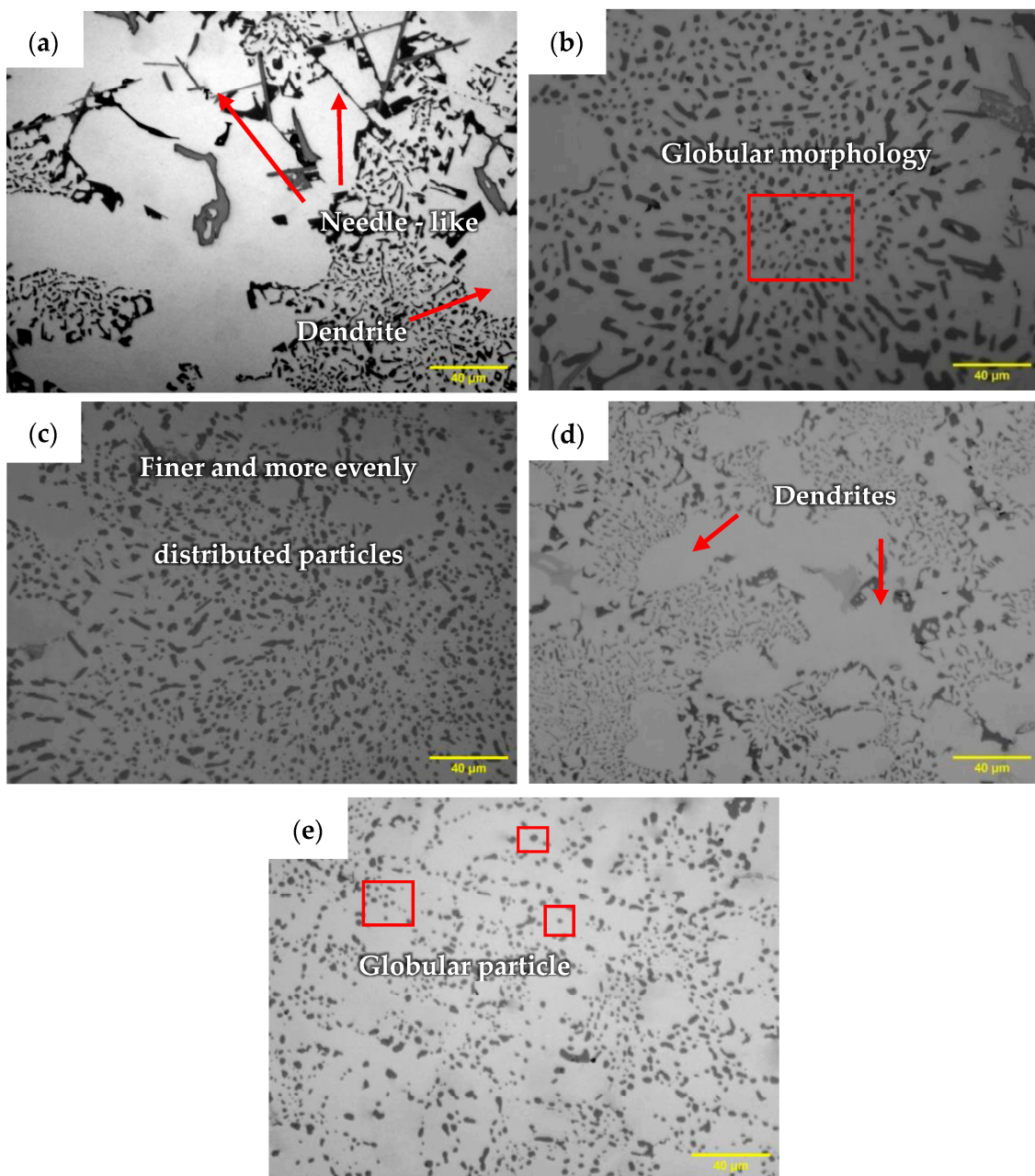

Figure 3. Photomicrographs of AA4032 samples under the following conditions: (**a**) As-cast, (**b**) HT, (**c**) HT-Rolled, (**d**) Forged and (**e**) HT-Forged.

The effect of the solubilized heat treatment on microstructure was evident, as is shown in Figure 3b, where it was observed that the distribution of eutectic silicon was more homogeneous in addition to a change from its normal needle-like morphology to a more globulized morphology, solely by the effect of strontium addition in the molten state. This effect has been discussed by Tebib et al. [16]. In a practical way, the percentage of eutectic silicon transformation can be improved by having longer heat treatment times or even slightly increasing the concentration of Sr to potentiate this effect.

The microstructure shown in Figure 3c corresponds to the HT-Rolled sample subjected to a reduction of the original thickness of 25%. In this micrograph, it can be seen that the acicular eutectic silicon morphology transformed into finer [15] and more evenly distributed particles. Huie Hu et al. [13] found similar results under similar conditions of heat treating and rolling. Eutectic silicon particles become thinner as the degree of deformation increases, which is expected because the finer the grain, the more grain that act as "barriers" to stop dislocations or propagation of cracks. Therefore, the mechanical properties increase significantly.

Figure 3d shows a photomicrograph corresponding to the microstructure of the Forged part. The forging process allowed a successful deformation, achieving a reduction of 25% of the original thickness without suffering some type of cracking. In Figure 3d, it can be seen that, at first sight, the microstructure was modified in the sense of forging, where the main difference was that dendrites were much more elongated and narrower, contrary to what was observed in the microstructure shown in Figure 3a. This behavior was reflected in a slight increase in the mechanical properties.

The microstructure of Figure 3e corresponds to the HT-Forged sample; the change in the microstructure was perfectly observed, that is, the dendritic structure was refined, and the dispersion of the eutectic silicon particles was more homogeneous. Hard and brittle intermetallic particles did not accumulate at the grain boundaries, appearing more evenly distributed throughout the matrix [23]. This fact is reflected in an increase in the mechanical properties compared to the mechanical properties of the HT-Rolled sample. The transformation of the needle-like morphology of the eutectic silicon particles into globular particles was very similar to that of the HT-Rolled sample.

It is worth mentioning that all intermetallics were identified from the different samples by EDS in a way suggested by Belov, Hren and Shabestari [4,5,17]. As-cast aluminum alloys exhibit a wide variety of complex intermetallic phases formed during the solidification process. Due to its low solubility in the solid state, iron is one of the most common elements forming intermetallics in aluminum alloys. In the present case, this element forms the intermetallic phase $Al_8FeMg_3Si_6$, as can be seen in the micrograph of Figure 4a, which corresponds to the As-cast sample. The identification of these intermetallics agrees with the results reported by Sweet et al. [24]. In the same figure, other precipitates were also identified that most probably corresponded to Mg_2Si and Al_9FeNi.

Aluminum-silicon alloys containing magnesium will become suitable for heat-treating since the intermetallic compound Mg_2Si could be redistributed evenly. In this sense, the microstructure appearing in Figure 4b, which corresponds to the HT part, shows the intermetallic Mg_2Si particles in a dark tone. Agglomerates can be seen in the microstructure, which most probably corresponds to a combination of the intermetallics Al_2Cu, Al_7CuNi or $Al_8Mg_3Si_6$ [6].

As previously mentioned, the more the material is deformed, the more the microstructure will be refined. This can be seen in the microstructure shown in Figure 4c, which corresponds to the HT-Rolled sample, where practically all eutectic silicon particles acquired a rather globular morphology. In addition, eutectic silicon was easily identified in a gray tone and intermetallic Al_3Ni in a bright white tone.

The micrograph in Figure 4d corresponds to the Forged sample, where the typical microstructure of an As-cast part can be observed, i.e., high heterogeneity intermetallics in the shape of an elongated needle. In turn, the micrograph in Figure 4e corresponds to the HT-Forged, where the main change observed is the homogeneous distribution of the

elements throughout the matrix. In addition, the distribution of eutectic silicon was more homogeneous. In both micrographs Figure 4d,e, it is observed, to a lesser extent, some Ni, Mg, Fe and Cu rich intermetallics, constituting a mixture of phases, such as Al_9FeNi, Mg_2Si $Al_8FeMg_3Si_6$, $Al_5Cu_2Mg_8Si_6$ and, of course, eutectic silicon.
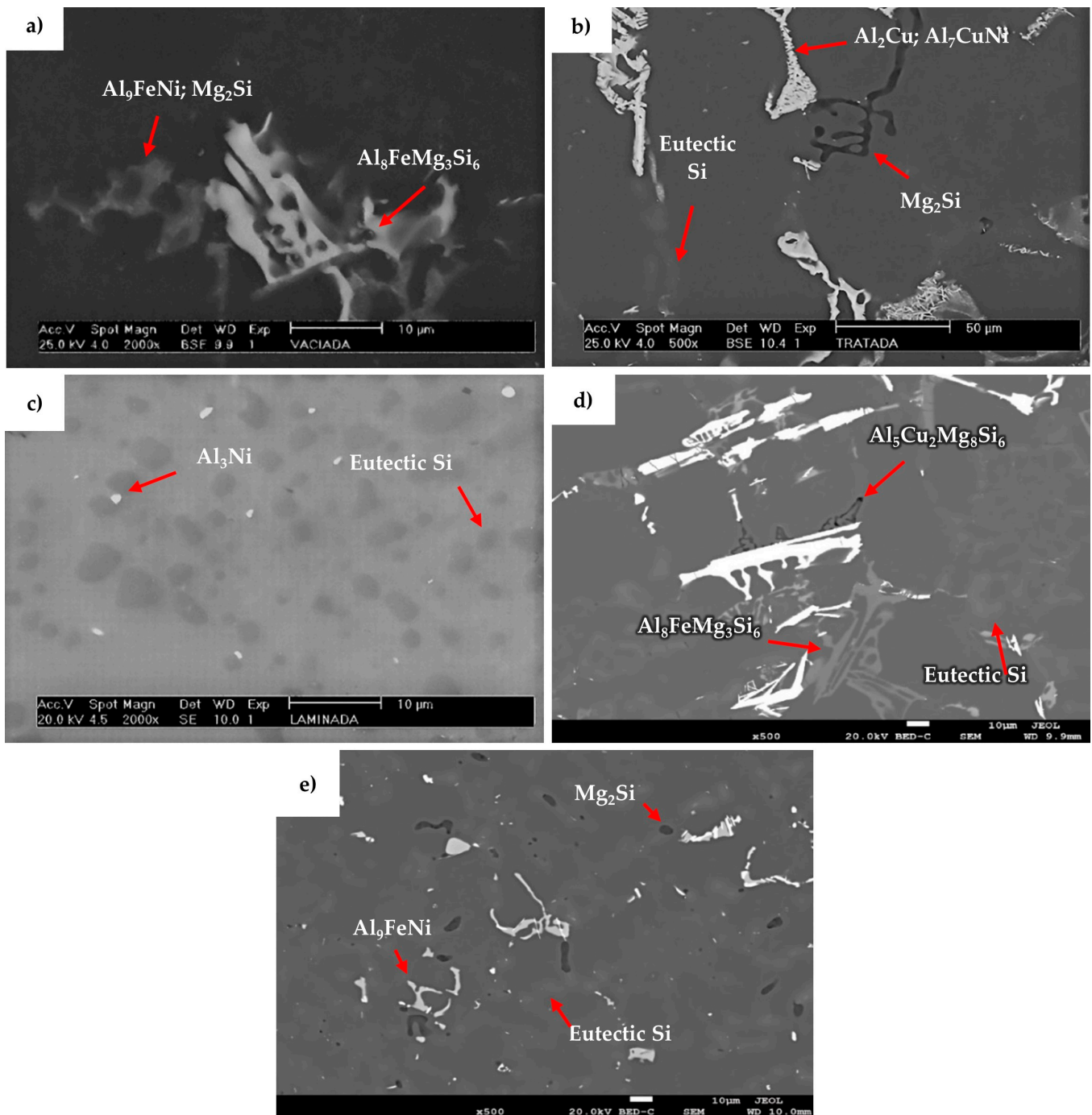

Figure 4. SEM micrographs showing the morphology of Mg_2Si particles and some major intermetallics of AA4032 under the following conditions: (**a**) As-cast, (**b**) HT, (**c**) HT-Rolled, (**d**) Forged, and (**e**) HT-Forged.

3.2. Mechanical Properties

The following is a summary of the results obtained on the mechanical properties measured for all samples studied in this work; there were 5 specimens in total, one for

each condition. The first result in Table 3 corresponds to the "As-cast" sample in which a maximum ultimate tensile stress (UTS) of 129 MPa and a yield strength (YS) of 110 MPa were observed, while its hardness Brinell (HB) was 55 units. The second value corresponded to the "HT" sample, which presented an UTS value of 200 MPa, a YS of 159 MPa and an HB of 40 units. In the case of the HT-Rolled sample, it reached a maximum tensile stress of 225 MPa, a YS of 180 MPa, and an HB of 77 units. As for the "Forged" sample, it reached a UTS value of 201 MPa, a YS value of 190 MPa, and an HB of 69.1 units. Finally, the HT-Forged sample reached an UTS value of 275 MPa, a YS value of 204 MPa, and an HB of 85.7 units. The last value reported in Table 3 corresponded to the properties reported in the literature for a commercial alloy in the 4xxx series [25].

Table 3. Comparison of the values of mechanical properties between alloys prepared from recycled materials vs. commercial purity alloys.

Sample	UTS (MPa)	YS (MPa)	Hardness (HB)
As-cast	129	110	55
HT	200	159	40
HT-Rolled	225	180	77
Forged	201	190	69.1
HT-Forged	275	204	85.7
4xxx series Commercial alloy	110–427	45–393	39–140

Table 3 summarizes all measured property values for the test conditions indicated; in general, intermediate values of UTS, YS and hardness were achieved, which were close to the values reported for commercial extruded alloys. Reaching higher values of mechanical properties would concern the degree of circularity of globulized eutectic silicon particles.

3.3. Circularity Analysis of Eutectic Silicon

The histogram distribution in Figure 5a is the result of the great heterogeneity of silicon, with a rather needle-like morphology, resulting in an average circularity of 0.44. The same figure shows that the distribution was mainly located in the left zone, which denotes minimal circularities corresponding to the As-cast sample. The frequency histogram in Figure 5b corresponded to the HT sample, where the average circularity increased considerably from 0.44 to 0.71. The frequency histogram was completely distributed to the right. For the HT-Rolled sample, whose histogram frequency is shown in Figure 5c, the average circularity of the eutectic silicon particles reached an average value of 0.74, with a histogram distributed to the right. The main difference was that some particles reached 0.89 of maximum circularity.

The results of Figure 5d correspond to the Forged sample, where the average circularity of eutectic silicon particles reached the value of 0.30. Figure 5e shows the results corresponding to the HT-Forged sample, where the average circularity of the eutectic silicon particles reached a circularity of 0.73. The frequency histogram included was distributed to the right, and a maximum circularity of 0.82 of the eutectic silicon particles was reached.

Table 4 summarizes the microstructural features calculated using ImageJ. The circularity was 0.44 in the As-cast sample, which was comprised of acicular eutectic silicon, as shown in Figure 3a. It is well known that silicon globulization can be accelerated by modifying the alloy with strontium [26].

Silicon modification is mainly promoted by the addition of strontium during the molten stage of the alloy. Strontium modification induces a high density of crystalline defects, effectively twinning the eutectic silicon and avoiding the growth of needle-like particles. Because of strontium addition in the heat-treated sample, the particles reached an average circularity of 0.71 and an average roundness of 0.65, as shown in Figure 3b and

summarized in Table 4. The reduction of the particle count is related to the dissolution of such particles during heat treatment [27].
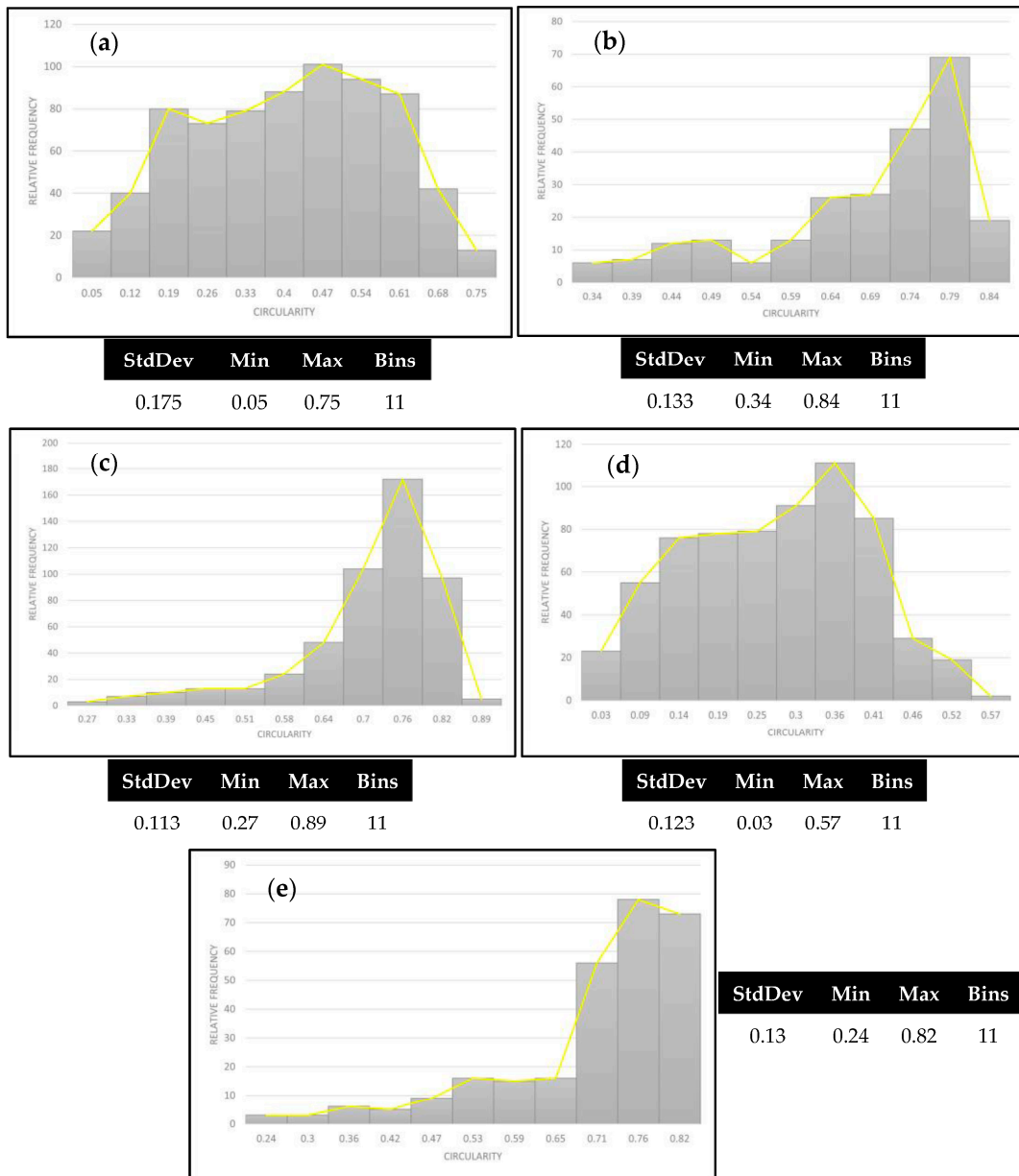

	StdDev	Min	Max	Bins
(a)	0.175	0.05	0.75	11
(b)	0.133	0.34	0.84	11
(c)	0.113	0.27	0.89	11
(d)	0.123	0.03	0.57	11
(e)	0.13	0.24	0.82	11

Figure 5. Histogram and frequency polygon of the silicon circularity analysis of the samples under the following conditions: (**a**) As-cast, (**b**) HT, (**c**) HT-Rolled, (**d**) Forged, and (**e**) HT-Forged.

Table 4. Summary of the characteristics obtained by the DIP.

Sample	Particle Number	Perimeter (μm)	Area (μm)^2	Roundness	Circularity
As-cast	719	9.42	2.77	0.51	0.44
HT	245	11.93	8.73	0.65	0.71
HT-Rolled	496	8.17	4.47	0.73	0.74
Forged	648	11.40	2.92	0.49	0.30
HT-Forged	280	8.65	5.14	0.69	0.73

A combined effect of deformation and modification can be appreciated in the HT-Rolled sample. Both circularity (0.74) and roundness (0.73) of this sample were the highest

of all the samples analyzed and can be corroborated in Figure 3c. It is believed that the defects caused by rolling act synergistically with strontium modification [26]. In contrast, the Forged sample displays the lowest values of circularity and roundness, as shown in Figure 3d and summarized in Table 4. This is probably related to the non-uniform strain caused by open forging as compared to the planar deformation induced by rolling [28].

3.4. Fracture Analysis

The fracture surface analysis of the As-cast sample subjected to the tensile test was analyzed by SEM, which showed a fracture of the ductile regime type. This can be verified because it presents an irregular surface with very marked valleys and crests, as can be seen in the micrograph of Figure 6a, which is characteristic of this type of fracture [29,30]. In the same figure, the dendritic structure, as well as a certain degree of porosity due to shrinkage, which act as small cavities that later coalesce into small cracks, is shown. Its mode of propagation perpendicular to the applied load generated the failure of the material.
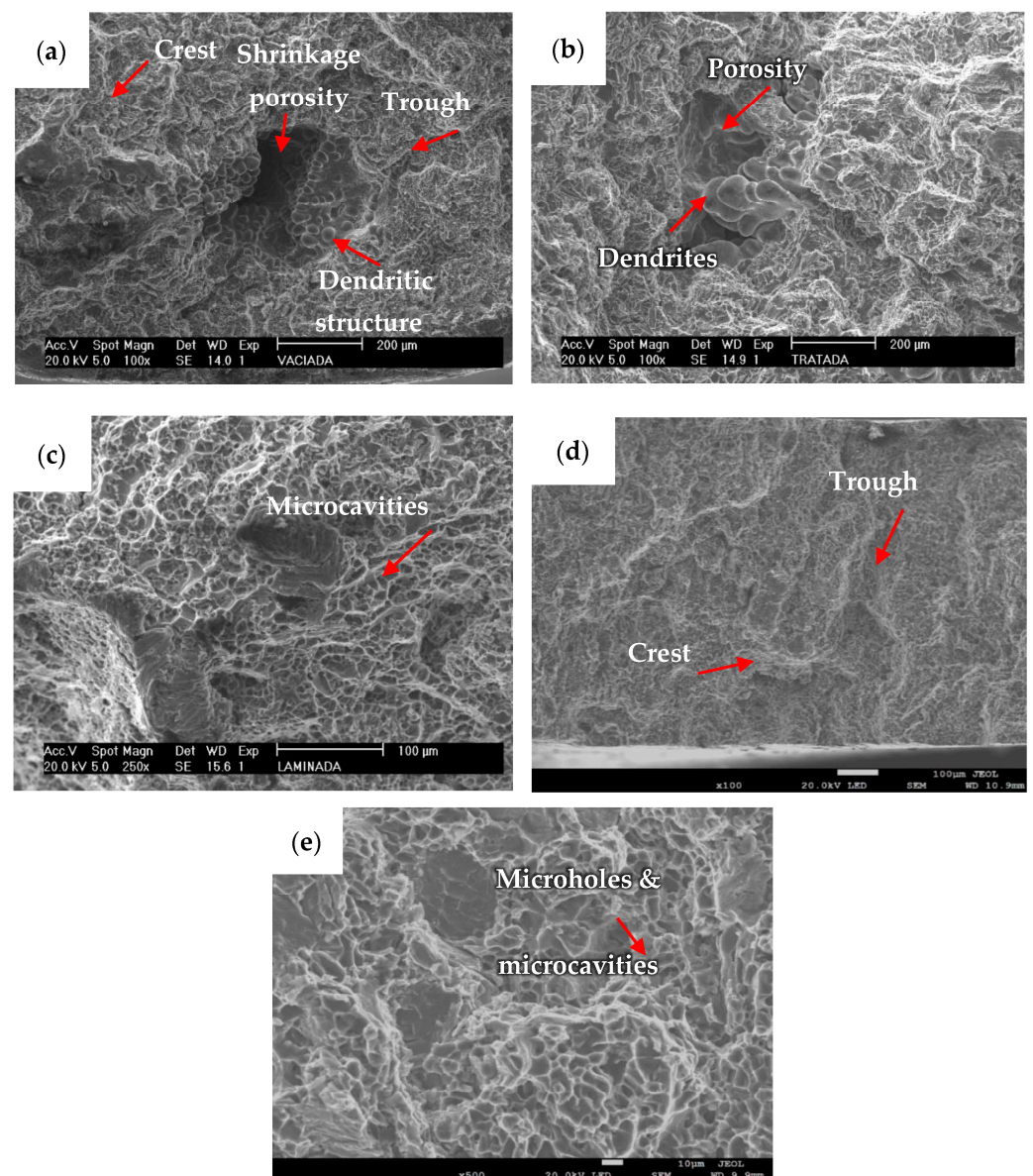
Figure 6. SEM micrographs of the fracture surface showing microcavities and microholes of AA4032 under the following conditions: (**a**) As-cast, (**b**) HT, (**c**) HT-Rolled, (**d**) Forged, and (**e**) HT-Forged.

The micrograph in Figure 6b corresponds to the fracture analysis of the HT sample, in which an irregular fracture surface with a certain degree of porosity was observed, corresponding to ductile fracture. The micrograph in Figure 6c corresponds to the HT-Rolled sample, where small fibrous cavities were also observed along the entire surface. This structure is characteristic of fracture caused by uniaxial tension, where each micro-cavity is half of a micro-dimple that was formed and then separated in the fracture process. Based on these features, it can be concluded that the sample presented a ductile fracture.

The surface fracture analysis of the Forged sample is shown in the micrograph of Figure 6d. The structures observed correspond to an irregular surface full of valleys and crests, but unlike the previous ones, which do not contain shrinkage of gas porosity defects, the mode of fracture corresponds to the ductile regime [31]. On the other hand, the micrograph in Figure 6e corresponds to the HT-Forged sample, which, in a very similar way to the previous image, shows a fracture mode within the ductile regime.

Hot processing by rolling and forging had an important effect on the microstructure and mechanical properties of the alloy. In general, the silicon corals were crushed, achieving a more homogeneous dispersion of silicon particles after plastic deformation.

The high temperature before rolling/forging in conjunction with plastic deformation caused a better diffusion of the atoms of the constituent elements, resulting in a more homogeneous composition, regardless of the increased density due to the holes being filled during plastic deformation.

4. Conclusions

1. All alloys prepared from recycled materials reached values of mechanical properties and hardness close to those of commercial alloys. Nevertheless, the mechanical properties could still be improved by applying some post-forging or rolling processes, such as aging.

2. The modification with Sr that acted directly on the eutectic silicon, the solubilized heat treatment and the rolling/forging processing together contributed to obtaining a more homogeneous and refined microstructure with which the mechanical properties improved considerably.

3. The circularity analysis was of great value since it was possible to quantitatively obtain the percentage of silicon transformation, achieving in some cases a transformation close to 90%, which was raised as a primary objective at the beginning of the work.

4. Regarding the open forging process, the results were quite positive, since the HT-Forged sample presented hardness, UTS and Ys values similar to those of the HT-Rolled sample. Considering the relative ease of carrying out this process, it is suggested that the open forge turned out to be a much more efficient process.

5. The fracture analysis showed that all samples presented a fracture within the ductile regime, caused mainly by the coalescence of microvoids in the constituent particles.

6. The chemical compositions of the processed alloy and the commercial alloy were quite similar. The only differences in the composition were Sr (0.04%) and Ti (0.10%) of the alloy type 4032 that was manufactured in the laboratory from aluminum scrap; therefore, it can be said that the alloy is within international specifications.

7. Finally, it can be concluded that the implementation of the forging or rolling process at an industrial level for the manufacture of small parts using 4032-type alloy prepared from scrap becomes an economically profitable and attractive process for future implementations and investigations.

Author Contributions: Conceptualization, F.A.G.P. and A.F.V.; Methodology, J.I.V.d.L.; Experimental design, J.I.V.d.L.; Data analysis, J.I.V.d.L.; Resources, F.A.G.P. and A.F.V.; Writing—original draft preparation, J.I.V.d.L.; Writing—review and editing, J.I.V.d.L., F.A.G.P. and A.F.V.; Visualization, J.I.V.d.L.; Supervision, F.A.G.P. and A.F.V.; Project administration, F.A.G.P. and A.F.V. All authors have read and agreed to the published version of the manuscript.

References

1. Li, Y.; Yue, Q.; He, J.; Zhao, F.; Wang, H. When will the arrival of China's secondary aluminum era? *Res. Pol.* **2020**, *65*, 101573. [CrossRef]
2. Dario, B.; Gianluca, B.; Davide, C.; Livan, F. Design of continuous friction stir extrusion machines for metal chip recycling: Issues and difficulties. *Proc. Manuf.* **2018**, *15*, 280–286. [CrossRef]
3. Eleonora, B.; Lorella, C.; Alessandro, M.; Andrea, M. En AW-4032T6 piston alloy after high-temperature exposure: Residual strength and microstructural features. *J. Mater. Eng. Perform.* **2017**, *26*, 3802–3812. [CrossRef]
4. Belov, N.; Eskin, D.; Avxentieva, N. Constituent phase diagrams of the Al–Cu–Fe–Mg–Ni–Si system and their application to the analysis of aluminium piston alloys. *Act. Mat.* **2005**, *53*, 4709–4722. [CrossRef]
5. Hren, I.; Svobodova, J.; Michna, S. Influence of Al5FeSi phases on the cracking of castings at Al-Si alloys. *Arc. Found. Eng.* **2018**, *18*, 120–124. [CrossRef]
6. Alberto, F.; Stefano, F.; Giulio, T. The influence of Sr, Mg and Cu addition on the microstructural properties of a secondary AlSi9Cu3(Fe) die casting alloy. *Mater. Character.* **2013**, *85*, 13–25. [CrossRef]
7. Rana, R.; Rajesh, P.; Das, S. Reviews on the influences of alloying elements on the microstructure and mechanical properties of aluminum alloys and aluminum alloy composites. *Int. J. Sci. Res. Pub.* **2012**, *2*, 1–7.
8. Jiang, J.; Yuan, T.; Shi, J.; Zhang, L.; Ma, A.; Song, D. Enhanced impact toughness ant ambient temperatures of ultrafine-grained Al-26 wt.% Si alloy produced by equal-channel angular pressing. *J. Mater. Eng. Perf.* **2018**, *27*, 2131–2137. [CrossRef]
9. Moslem, T.; Davood, R.; Armin, K.; Maryam, A. Investigation of annealing treatment on the interfacial and mechanical properties of Al5052/Cu multilayered composites subjected to ARB process. *J. Alloys Compd.* **2021**, *871*, 159513. [CrossRef]
10. Moslem, T.; Maryam, A.; Armin, K.; Davood, R.; Morteza, A.; Ramin, H. Effects of strain accumulation and annealing on interfacial microstructure and grain structure (Mg and Al$_3$Mg$_2$ layers) of Al/Cu/Mg multilayered composite fabricated by ARB process. *J. Mater. Res. Technol.* **2021**, *14*, 392–406. [CrossRef]
11. Hua, L.; Yuan, P.; Zhao, N.; Hu, Z.; Ma, H. Microstructure and mechanical properties of 6082 aluminum alloy processed by preaging and hot forging. *Trans. Nonferrous Met. Soc. Chin.* **2022**, *32*, 790–800. [CrossRef]
12. Tao, H.; Gang, Z.; Ni, T.; Fuxiao, Y.; Liang, Z. Deformability of eutectic Al-Si alloys produced by semi-continuously DC casting during hot-rolling. *Mater. Sci. Forum.* **2012**, *706–709*, 436–440. [CrossRef]
13. Peng, S.; Hongfu, Y.; Rensong, H.; Yelin, Z. The effect of rolling temperature on the microstructure and properties of multi pass rolled 7A04 aluminum alloy. *J. Mater. Res. Technol.* **2023**, *25*, 3200–3211. [CrossRef]
14. Wang, Y.; Liao, H.; Wu, Y.; Yang, J. Effect of Si content on microstructure and mechanical properties of Al-Si-Mg alloys. *Mater. Desig.* **2014**, *53*, 634–638. [CrossRef]
15. Hu, H.; Kong, X.; Shao, Z.; Wang, X. Thermoplastic deformation behavior of 4032 Al alloy. *Adv. Mater. Res.* **2011**, *393–395*, 481–484. [CrossRef]
16. Tebib, M.; Samuel, A.; Ajersch, F.; Chen, X.-G. Effect of P and Sr additions on the microstructure of hypereutectic Al-15Si-14Mg-4Cu alloy. *Mater. Character.* **2014**, *89*, 112–123. [CrossRef]
17. Shabestari, S.; Gholizadeh, R. Assessment of intermetallic compound formation during solidification of Al–Si piston alloys through thermal analysis technique. *Mater. Sci. Technol.* **2012**, *28*, 156–164. [CrossRef]
18. Wilhelm, B.; Mark, B. *Principles of Digital Image Processing: Fundamental Techniques*, 9th ed.; Springer: Berlin/Heidelberg, Germany, 2009.
19. Sean, G. *Digital Image Processing and Analysis with ImageJ*; Wiley Interscience: Hoboken, NJ, USA, 2010.
20. Tiago, F.; Wayne, R. *The ImageJ User Guide*; Version IJ1.43r; 2010.
21. David, W. On optical and data-based histograms. *Biometrika* **1979**, *66*, 605–610. Available online: http://www.jstor.org/stable/2335182 (accessed on 2 September 2022).
22. Cho, Y.H.; Joo, D.H.; Kim, C.H.; Lee, H.C. The effect of alloy addition on the high temperature properties of over-aged Al-Si (CuNiMg) cast alloys. *Mater. Sci. Forum.* **2016**, *519-521*, 461–466. [CrossRef]
23. Alexandre, G.; Oleg, S.; Taku, S.; Rustam, K.; Hiromi, M. Grain refinement in as-cast 7475 aluminum alloy under hot equal-channel angular pressing. *Mater. Trans.* **2003**, *44*, 766–774.
24. Sweet, L.; Zhu, M.; Gao, S.; Taylor, J.; Easton, M. The effect of iron content on the iron-containing intermetallic phases in a cast 6060 aluminum alloy. *Metall. Mater. Trans. A* **2013**, *42*, 1737–1749. [CrossRef]
25. ASM International. Properties and selection: Nonferrous alloys and special purpose materials. In *ASM International Handbook*, 10th ed.; ASM International: Almere, The Netherlands, 1992; Volume 2.
26. Nima, H.; Abbas, Z.-H.; Megumi, K.; Andre, B.; Peter, D. Effect of severe plastic deformation and subsequent silicon spheroidizing treatment on the microstructure and mechanical properties of an Al–Si–Mg alloy. *Adv. Eng. Mater.* **2017**, *19*, 1700064. [CrossRef]

27. Ibrahim, M.; Abdelaziz, M.; Samuel, A.; Doty, H.; Samuel, F. Spheroidization and coarsening of eutectic Si particles in Al-Si-based alloys. *Adv. Mater. Sci. Eng.* **2021**, *21*, 6678280. [CrossRef]

28. Wang, J.; Zhu, J.; Liu, Y.; Peng, H.; Su, X. Effect of spheroidization of eutectic Si on mechanical properties of eutectic Al–Si alloys. *J. Mater. Res.* **2018**, *33*, 1773–1781. [CrossRef]

29. Antonio, F.; Enric, M.; Baile, M. Propiedades mecánicas y análisis fractográfico de componentes de aluminio conformados en estado semisólido. *Anal. Mec. Fract.* **2007**, *1*, 93–98.

30. Pahlavani, M.; Marzbanrad, J.; Rahmatabadi, D.; Hashemi, R.; Bayati, A. A comprehensive study on the effects of heat treatment on the fracture behaviors and structural properties of Mg-Li alloys using RSM. *Mater. Res. Express.* **2019**, *6*, 076554. [CrossRef]

31. Manel, S.; José, R.-I. Estudio del crecimiento de grieta a fatiga en la aleación de aluminio A357 producida mediante new rheocasting. *Anal. Mec. Fract.* **2005**, *22*, 167–172. Available online: https://www.researchgate.net/publication/242624916 (accessed on 21 May 2020).